Field- and geometry-controlled avoided crossings of spin-wave modes in reprogrammable magnonic crystals

Jesco Topp, Stefan Mendach, and Detlef Heitmann
Institut für Angewandte Physik und Mikrostrukturforschungszentrum, Universität Hamburg, Jungiusstrasse 11, D-20355 Hamburg, Germany

Mikhail Kostylev
School of Physics, M013, University of Western Australia, 35 Stirling Hwy, 6009 Crawley, Western Australia, Australia

Dirk Grundler*
Lehrstuhl für Physik funktionaler Schichtsysteme, Technische Universität München, Physik Department, James-Franck-Str. 1, D-85747 Garching b. München, Germany

(Received 4 October 2011; revised manuscript received 30 October 2011; published 7 December 2011)

We study the spin dynamics in arrays of densely packed submicron $Ni_{80}Fe_{20}$ wires which form one-dimensional magnonic crystals. They are subject to an in-plane magnetic field H being collinear with the wires. In the case when neighboring wires are magnetized antiparallel, broadband spin-wave spectroscopy reveals a mode repulsion behavior around a certain field H_{mr}. We attribute this to dipolar coupling and avoided crossing of resonant modes of individual wires. The modes are found to hybridize across the array and form acoustic and optical modes. When an array of alternating-width wires is considered, H_{mr} is found to vary characteristically as a function of the width difference Δw of neighboring wires. Interestingly, the sign of H_{mr} reflects the orientation of the wires' magnetization. For our devices we find experimentally frequency splittings δf on the order of 1 GHz between the acoustic and optical mode. We use micromagnetic modeling to analyze spin precession profiles and investigate the hybridization of modes. The simulated splitting is larger than the observed one. We attribute the discrepancy to a reduced dipolar coupling in the real samples. Using a theoretical model which considers the reduced dipolar coupling we analyze δf for different geometrical parameters such as the edge-to-edge separation a and the width difference Δw. Though relevant for H_{mr}, Δw is not decisive for δf. Instead, a is key for the frequency splitting. The results are relevant in order to tailor the dynamic response and band structure of magnonic crystals.

DOI: 10.1103/PhysRevB.84.214413 PACS number(s): 75.75.−c, 76.50.+g, 75.30.Ds, 75.78.−n

I. INTRODUCTION

Nanostructuring of materials allows one to form cavities and confine different kinds of waves such as electromagnetic, plasmon, or spin waves depending on the material properties. The usual strategy to tune the frequency of a cavity-based oscillator is to vary its geometry which in turn varies the wavelength of a standing wave in the cavity. For spin waves the patterned magnet itself functions as a cavity. The resonance can be tuned not only by the specific geometry,[1] but also by varying the magnetization,[2] the applied magnetic field,[3] and magnetic history.[4] Importantly, nanomagnets represent resonators of open type, which means that their fields are not confined completely inside the magnetic material: A significant microwave magnetic field is present also in the space around them. This allows for coupling of neighboring oscillators and formation of collective spin-wave (magnonic) modes in periodic arrays of such elements. For the latter property periodic arrays of magnetic nanoelements are termed magnonic crystals (MCs).[5] Recently, a periodic array of densely packed magnetic nanowires has been found to form an MC where the band structure is reprogrammed by the in-plane magnetic field H.[6] In the long wavelength limit (i.e., for small wave vectors k), a field-dependent mode repulsion with a frequency splitting $\delta f \approx 1$ GHz has been observed around $H = 0$ when neighboring wires experienced an antiferromagnetic order (AFO). Following Ref. 6 this frequency splitting δf is a measure of the bandwidths of the two lowest allowed magnonic minibands in case of symmetric nanowires. The microscopic origin of the frequency splitting and its characteristic field dependence was not discussed. Only very recently Ding *et al.* presented a thorough study on dipolar coupling of short nanowires. They reported a hybridization of modes where, both the static and dynamic dipolar coupling governed the eigenfrequencies and field dependencies.[7] The dynamic response was found to be very sensitive to the width difference Δw of neighboring wires. However, the upper mode of the field-dependent mode repulsion observed earlier in Ref. 6 did not show up experimentally (cf. Fig. 1 in Ref. 7). Further studies are needed to elucidate the hybridization of coupled oscillators in magnonic crystals. In this paper we investigate very long nanowires with, in particular, $\Delta w \neq 0$ where static dipolar coupling is not decisive. Using broadband spin-wave spectroscopy, micromagnetic simulations, and further theoretical modeling we find that the dynamic dipolar coupling leads to the experimentally observed repulsion of two modes which we attribute to a field-controlled avoided crossing due to hybridized magnonic excitations. We find that the frequency splitting δf to depend crucially on the edge-to-edge separation a but not on the width difference Δw. The findings are important for magnonics[8] where one aims at tailoring allowed minibands and frequency gaps in MCs.

This paper is organized as follows. In Sec. II we describe the experimental techniques that we used to fabricate and investigate the nanowire arrays. Section III outlines the micromagnetic modeling and theoretical approaches. Experimental

results obtained for major and minor hysteresis loops are presented in Sec. IV. In Sec. V we perform data analysis and compare the experimental data with theoretical results. We conclude in Sec. VI.

II. EXPERIMENTAL TECHNIQUES: NANOLITHOGRAPHY AND SPIN-WAVE SPECTROSCOPY

Nanowire arrays were prepared on semi-insulating substrates. We used substrates of either [100] Si covered with 300-nm thick SiO_2 or [100] GaAs. Both substrates provided excellent surface quality and a high dielectric constant. A PMMA 50k/950k double-layer resist and thermal evaporation of $Ni_{80}Fe_{20}$ (Permalloy) were utilized to create nanowires by lift-off processing.[6,9–11] In this paper we will discuss in detail sample A. A sketch and a scanning electron microscopy (SEM) image of this sample are shown in Fig. 1. Sample A consists of 200 pairs of 160-μm-long wires with alternating widths $w_1 = 370$ nm, $w_2 = 315$ nm, and an edge-to-edge separation of $a = 100$ nm. Due to the shape anisotropy the magnetization $\mathbf{M}$ of each wire aligns preferentially with the long (easy) axis of the wire. The wires are thus bistable. The width difference $\Delta w = w_1 - w_2$ is just 55 nm (i.e., the widths differ by a factor of only 1.17). The width difference is smaller by an order of magnitude if compared to the MC considered in Ref. 12 and similar to the study performed on short nanowires.[7] Atomic force microscopy reveals a thickness of $t = 25$ nm for sample A. The saturation magnetization is $\mu_0 M_s = 1.02$ T as determined from a ferromagnetic resonance characterization of an unpatterned reference film. All *wide* wires are interconnected at one end via a 5-μm-wide orthogonal stripe [Fig. 1(c)]. A

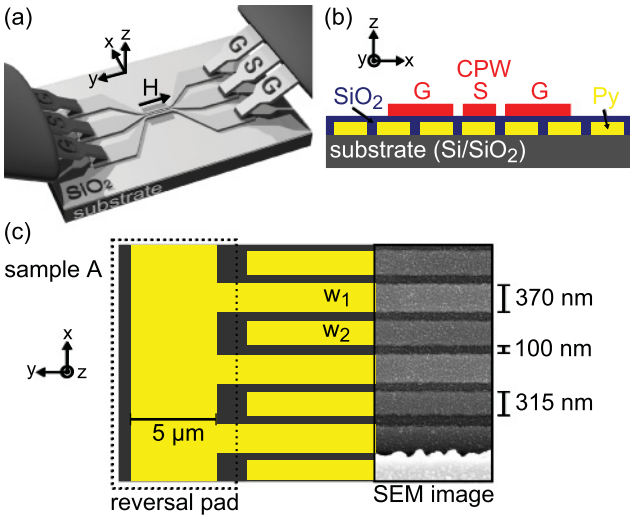

FIG. 1. (Color online) (a) Sketch of the experiment. The nanowire array is located underneath a coplanar waveguide with two ground (G) and one signal line (S). (b) Side view of a sample showing the layered structure. (c) Layout and SEM image of sample A. Each period of this structure contains two wires of different widths. The difference in wire widths is $\Delta w = 55$ nm. Note the presence of a reversal pad for sample A. Its purpose is to narrow the distribution of the the switching fields for the wide wires. The bright area in the SEM image is a part of the CPW (bottom at the right).

50 Ω coplanar waveguide (CPW) on top of the ferromagnetic sample is used to excite and detect spin waves [Fig. 1(a)]. The CPW's central conductor is 10-μm wide and is oriented parallel to the wires long axis, that is, along the easy-axis direction [Fig. 1(b)]. The CPW was fabricated using electron beam lithography. We utilized a PMMA 600k resist and thermal evaporation of a 150-nm-thick trilayer of Cr/Ag/Au. The ferromagnetic wires and CPW are electrically isolated from each other by a 100-nm-thick layer of SiO_2. We use a vector-network analyzer (VNA) as a source and a detector in a broadband spin-wave spectroscopy experiment.[13,14] The VNA measures the transmission of microwaves from 10 MHz to 26.5 GHz through the CPW with an accuracy of 0.5×10^{-3} dB. We apply a small microwave power of -10 dBm to ensure the linear regime of spin-wave excitation. At such a low power the magnetic rf field amplitude around the CPW is smaller than 0.1 mT which is well below the onset of nonlinear effects.[10,15,16] Our study is thus different from Ref. 17 where nonlinear hybridization was addressed. When the microwave frequency matches the eigenfrequency for a spin-wave resonance a drop in the transmission is observed. This is caused by resonant absorption of microwave power by the precessing magnetization $\mathbf{M}$ due to the torque $\tau \propto \mathbf{M} \times h_{rf}$ where h_{rf} is the microwave magnetic field. We normalize each spectrum by a reference spectrum obtained at a field of 90 mT applied in a direction perpendicular to the wires. Here τ is at a minimum and the frequency-dependent response of the CPW itself is measured. By this means we increase the signal-to-noise ratio of spin-wave resonances.[13] As the CPW width is 10 μm and large compared to the periods of the arrays we probe long-wavelength spin waves (i.e., ones with wave numbers close to $k = 0$). Spectra are taken using the measurement protocol as follows: (i) A magnetic field is applied to define the magnetic history; (ii) the "measurement" field H is applied parallel to the wires; (iii) the microwave transmission $T(f)$ is measured; (iv) a reference field of $+90$ mT is applied perpendicular to the wires; (v) the reference transmission $T_r(f)$ is measured; (vi) the ratio $T(f)/T_r(f)$ is calculated. Steps (i)–(vi) are repeated for different H. We note that the excitation is not completely zero in step (iv) as the microwave field couples weakly to edge modes of the wires. We have chosen a moderate value of $+90$ mT as a reference field to position the corresponding resonance frequency below the frequency regime taken by the avoided crossing addressed in the present paper.

III. THEORETICAL APPROACHES AND MODELING

To develop an understanding of the mode repulsion and field-dependent avoided crossing it is instructive to start the theoretical analysis from a phenomenological analytical model for uncoupled wires. For this we calculate eigenfrequencies f following the formalism of Ref. 18. This theory assumes that a standing spin wave is formed across the wire width due to the geometrical confinement. As a result of the confinement the wave vector k_t which is directed perpendicular to the wire edges is quantized. The standing waves are Damon-Eshbach (DE) spin waves whose behavior in the confined geometry is strongly affected by the dynamic demagnetization. The demagnetization introduces an effective dipolar pinning of

the dynamic magnetization at the edges. The strength of the effective pinning determines the discrete values of k_t for the standing waves. Depending on the width w the value k_t changes and thereby the eigenfrequency.

Furthermore we use micromagnetic simulations to shed more light on the excitations in the coupled nanowires. The simulations are based on the OOMMF software.[19] The material parameters are $\mu_0 M_s = 1.02\,\mathrm{T}$, $A = 13 \times 10^{-12}\,\mathrm{J/m}$ (exchange constant), and $\gamma = 176\ \mathrm{GHz/T}$ (gyromagnetic ratio). We approximate our sample A by considering 15 unit cells each of which consists of two wires with in-plane sizes extracted from scanning electron microscopy and atomic force microscopy images. A larger number of unit cells does not change the simulation results. The simulated segment has a dimension of $\Delta x \times \Delta y \times \Delta z = 13276 \times 4 \times 24\ \mathrm{nm}^3$. It is discretized in cells of $4 \times 4 \times 4\ \mathrm{nm}^3$. The segment is continued periodically in the y direction using periodic boundary conditions.[20] The wires are thus assumed to be infinitely long in the y direction such that static dipolar fields do not play a role. The direction of **M** for each of the 30 simulated wires is set prior to the simulation in agreement with the ferromagnetic order (FMO) and AFO states. The spin precession is excited by a field pulse with $\mathbf{h}_{\mathrm{rf}} = (0.7,0,0.7)\,\mathrm{mT}$. The full width at half maximum of the pulse is 2.5 ps. Fast-Fourier transformation of the time evolution of M results in a spectra of frequencies of eigenexcitations. For this the simulation time covers a time period of 5 ns after which the precession amplitude is almost zero due to damping and allows for artefact-free zero padding to 21 ns. We analyze the time-dependent data starting from 0.5 ns after the pulsed excitation. Such data also provide us with spatial profiles of the eigenmodes. Field dependencies of the eigenfrequencies and spin-precession profiles are extracted from the spin dynamics for the innermost unit cell to avoid boundary effects.[11] Because of the large ellipticity of precession in thin metallic films we make use of the in-plane component of dynamic magnetization for the illustration purposes.

A more detailed theoretical analysis will be performed using the numerical model from Ref. 12. This software numerically solves an eigenvalue problem for an integro-differential equation. This equation follows from the linearized Landau-Lifshitz-Gilbert equation. This equation is derived specifically for the quasi-one-dimensional geometry of a periodic array of parallel nanowires of infinite length. The modeling is thus efficient to analyze the formation of the avoided crossing and frequency splitting for a broad range of parameters. In contrast to the standard OOMMF software the integro-differential equation model is formed to incorporate a parameter l_c which can account for a reduced strength of the dipolar coupling. The approach thus includes a phenomenological parameter which corresponds to the length over which the dipolar coupling in the array is effective. The physical meaning of this parameter is the distance between the source of the dynamic dipole field and the point of its observation at which the strength of dipolar coupling is reduced by a factor of $1/e$ due to imperfections of the real sample if compared to the ideal one. The value of l_c is extracted by fitting experimental data with the model. For further details we refer to Ref. 5. Originally the parameter was called "coherence length" when used to describe the results of Brillouin light scattering experiments where data showed systematically smaller bandwidths of the allowed miniband at low frequency if compared with a modeling assuming long-range dipolar coupling over the whole array. In the case of all-electrical spin-wave spectroscopy at long wavelengths or ferromagnetic resonance experiments it is instructive to call this parameter "dipolar coupling length," as the phase coherence of precession is imposed by the uniformity of the microwave driving field.

IV. SPIN-WAVE SPECTRA FOR MAJOR AND MINOR HYSTERESIS LOOPS

For an array of q bistable wires, each of which is magnetized uniformly, in principle 2^q different magnetization configurations (magnetic ground states) are possible. We discuss only two periodic arrangements, that is, the ferromagnetic order, for which magnetization vectors **M** in all wires are aligned in the same direction, and the antiferromagnetic order, for which neighboring wires are magnetized antiparallel. These configurations are sketched in Fig. 2(a) and can be set by a tailored magnetic field history in step (i) of the measurement protocol. This has been demonstrated in Ref. 6. Disordered states of nanowire arrays have been addressed in Ref. 21 recently. To improve the degree of ordering for

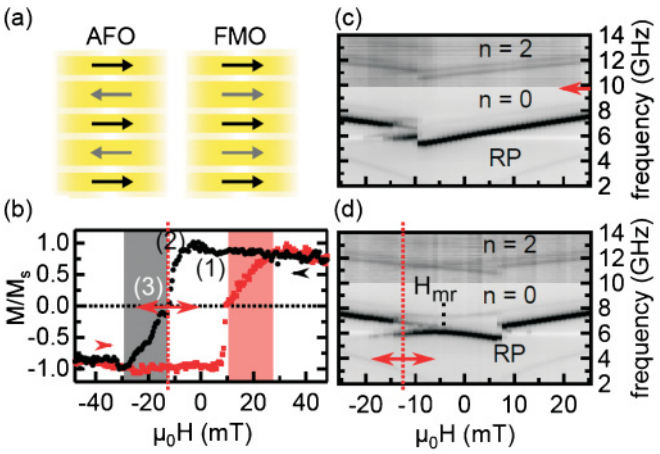

FIG. 2. (Color online) (a) Illustration of antiferromagnetic (AFO; left) and ferromagnetic order (FMO; right). Arrows mark the direction of **M** for each wire. (b) Magnetic hysteresis for sample A. Small arrows mark the sweep directions when taking the MOKE data. Spin-wave spectra (grayscale plots) of sample A obtained (c) after initial saturation at +50 mT parallel to the wires and (d) after applying +50 mT and −12 mT. For $-12\ \mathrm{mT} < \mu_0 H < +8\ \mathrm{mT}$ the AFO is stable. In this field regime the spectra of (c) and (d) are markedly different. Dark color in (c) and (d) represents absorption. In (d) we indicate H_{mr} for mode $n = 0$ (i.e., the position of the frequency maximum of the intense low-frequency mode). Above 10 GHz the contrast has been enhanced. The horizontal white lines at 5.9 GHz in (c) and (d) reflect the excitation of the edge modes at the reference field of +90 mT applied perpendicular to the wires. Since all data are normalized to the same reference data set the edge excitation shows up as a constant white line. The vertical dotted line in (b) indicates the starting field of −12 mT when taking spectroscopy data shown in (d). We replot the vertical dotted line in (d). The horizontal large arrows in (b) and (d) indicate the two different sweep directions when taking the spectroscopy data shown in (d).

the AFO state, sample A is equipped with the 5-μm-wide reversal pad (RP). This RP is introduced to synchronize the magnetization reversal of the wide wires and to narrow the distribution of switching fields. In Fig. 2(b) we show the hysteresis loop of sample A. This is obtained by measuring the longitudinal magneto-optical Kerr effect (MOKE). The laser-spot diameter is about 100 μm such that the data reflect the magnetic behavior averaged over many periods of the array. The hysteresis loop is subdivided into three regimes: (1) magnetic saturation, (2) a narrow field region with a sharp drop in the magnetization, and (3) a wide region where the total magnetization of the sample varies gradually as a function of H. Coming, for example, from positive H the total magnetization remains constant at $M/M_s = +1$, that is, the array is in the FMO state. This state holds down to $\mu_0 H \approx -10$ mT. Then a relatively sharp jump occurs ending at M/M_s slightly below zero. This irreversible process represents the switching of a large number of wires. Between -10 mT and -25 mT (shaded region) the magnetization varies monotonously until saturation at $M/M_s = -1$ is reached. This kind of hysteresis loop has previously been reported for a wire array in Ref. 22. The irreversible process in the narrow field regime around -10 mT is attributed to the wide wires attached to the RP which supports synchronized domain nucleation for the wires reversal. The AFO state is formed in this way. The narrow wires switch at larger magnitudes of the applied field and do so over a wider field range, owing to the statistical distribution of the individual switching fields. Obviously, the AFO state with a high degree of antiferromagnetic ordering of neighboring nanowires is at the low-field sides of the shaded regions (i.e., right after the sharp jump in the hysteresis curve).

Spin-wave spectra obtained when decreasing the applied field from positive saturation at $+50$ mT are displayed in Fig. 2(c). For fields larger than -10 mT we observe three families of resonance peaks. These are labeled RP, $n = 0$, and $n = 2$. The resonance at very low frequency is consistent with the one for a transversely magnetized 5-μm-wide magnet.[23] This peak is attributed to the RP. This resonance is not relevant to our study and will not be discussed in the following. In the FMO state at $\mu_0 H > -10$ mT each of the families $n = 0$ and $n = 2$ consists of a pair of resonances. One sees that in each pair the lower-frequency peak is of significantly larger intensity than the higher-frequency one. At -10 mT we observe a discontinuous jump in the frequencies of both pairs. This field is consistent with the synchronized switching field of the wide wires, as extracted from the MOKE data [Fig. 2(b)]. Thus, this jump marks the transition to the AFO state. (Note that, consistently, at nearly the same field the resonance of the RP regains a large intensity for decreasing H.) For -20 mT $< \mu_0 H < -10$ mT the spectra are richer in Fig. 2(c). We find branches with opposite slopes $\partial f/\partial H$ as a function of H (i.e., positive and negative $\partial f/\partial H$). Below -20 mT the two resonance pairs $n = 0$ and $n = 2$ are visible again. They have a common slope $\partial f/\partial H$ and a behavior which is mirrored if compared to the data at large positive H. This behavior is thus consistent with the reversed FMO state.

We now study in detail the AFO state. To this end we perform a measurement inside a minor hysteresis loop. After first saturating the sample in the magnetic field $+50$ mT and then decreasing the field down to -12 mT, the sample is set to the AFO state. The data taken after this magnetization history [Fig. 2(d)] look markedly different from Fig. 2(c). The largest difference is observed for the field range -12 mT $< \mu_0 H <$ $+8$ mT, where one observes extra branches whose frequencies vary nonmonotonously with the applied field in Fig. 2(d). The nonmonotonic behavior of resonance frequencies is consistent with the AFO ground state.[6,12] This suggests that the AFO state is stable over this field range. At $+8$ mT we observe a discontinuous jump in the spin-wave frequencies and for larger fields the two pairs $n = 0$ and $n = 2$ are found which exhibit the same positive slope $\partial f/\partial H$. This indicates the transition to the FMO state at $+8$ mT. For fields below -20 mT we find the reversed FMO state.

From comparison of Figs. 2(c) and 2(d) it becomes evident that the AFO state is characterized by a very specific shape of $f(H)$ dependence. The main feature of this dependence is the nonmonotonic character with extrema for each branch near $H = 0$ (either a minimum or a maximum). The lowest branch (with the largest intensity) has a negative curvature and a maximum frequency of $f = 5.95$ GHz which is found at $\mu_0 H_{mr,0} = -5$ mT. The higher-frequency mode of weak intensity of the resonance pair $n = 0$ has a positive curvature and a frequency minimum of 7.2 GHz at $\mu_0 H_{mr,0}$. In Ref. 6 this behavior was identified as a mode repulsion. At -5 mT the frequency splitting amounts to $\delta f = 1.25$ GHz. The small signal-to-noise ratio and the finite linewidth of the resonances which belong to the resonance pair $n = 2$ do not allow us to infer, whether branches of opposing slope cross or repulse at $\mu_0 H_{mr,2} = -9.5$ mT. A detailed analysis of Fig. 2(d) shows that the AFO state is not perfect at -12 mT. There is a further weak mode for $\mu_0 H < -5$mT which merges with the FMO branch at large negative fields. We attribute this to some parasitic FMO domain similar to the one recently observed in Ref. 21.

For comparison and reference we consider now experimental results obtained on further nanowire arrays. One array (sample B) was fabricated on GaAs and consisted of 450 180-μm-long wires with $w = w_1 = w_2 = 300$ nm. Thus sample B exhibited $\Delta w = 0$. The edge-to-edge separation $a = 100$ nm was the same as for sample A. Its thickness was $t = 20$ nm and saturation magnetization $\mu_0 M_s = 1.12$ T. Spectra obtained on sample B were presented in detail in Ref. 6 and will not be repeated here. For this sample we observed a mode repulsion in the AFO state with $\delta f = 1.05$ GHz for the pair $n = 0$. The value was found near $\mu_0 H_{mr,0} \approx -1$ to -2mT. A further sample consisted of 10 $w = 300$-nm-wide wires with a large separation $a = 700$ nm. Its thickness was $t = 20$ nm and $\mu_0 M_s = 1.11$ T. Such a device was utilized as a reference sample. The large separation and small number of wires reduced the dipolar interaction to a minimum. It did not exhibit the interaction effects considered in this paper and will therefore not be discussed further.

V. DATA ANALYSIS AND DISCUSSION

We now discuss the microscopic origin of the mode repulsion observed as a function of in-plane field H in the AFO state. We will start with a phenomenological analytical model for *uncoupled* wires (i.e., uncoupled oscillators). Then we will present the micromagnetic simulations where the

long-range dipolar *coupling* is included. In the last part of the section we discuss the solution of an eigenvalue problem for an integro-differential equation which is derived from the linearized Landau-Lifshitz-Gilbert equation. Here we consider a reduced dipolar coupling strength.

A. Results from the analytical model

In Fig. 3(a) we show eigenfrequencies f calculated for the two uncoupled nanowires of different widths $w_1 = 370$ (black curves) and $w_2 = 315$ nm (gray curves) following Ref. 18. The full (broken) lines are for wires where **M** points in the right (left) direction. Here, we assume that a positive field H points to the right. We show data for two different eigenmodes $n = 0$ and $n = 2$. The integer number n equals the number of nodal planes which extend along the long axis of the wire. We find that a mode with $n = 0$ (i.e., the fundamental mode) is about 5 GHz below a mode with $n = 2$. For every mode order n the narrow wire exhibits an eigenfrequency which exceeds the respective frequency for the wide wire by about 0.5 GHz. The difference in eigenfrequencies is consistent with experimental data obtained on noninteracting nanowires of different width.[11]

Consider now a periodic array with alternating-width nanowires. If there is no dynamic dipolar coupling between the wires of different widths the eigenfrequencies of Fig. 3(a) are still a solution for such an array. If static magnetization vectors for all wires are co-aligned the resonances in the two different types of wires are well separated in frequency. They shift in parallel as a function of the field H and do not cross (full lines in the figure). The respective FMO configuration is

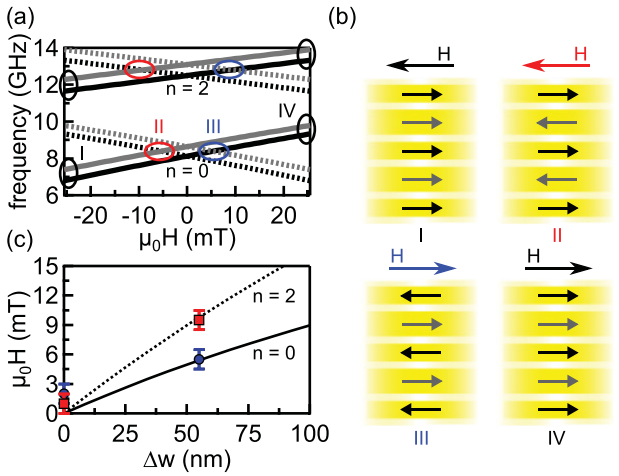

FIG. 3. (Color online) (a) Field dependence of eigenfrequencies of individual nanowires with $w_1 = 370$ nm (black lines) and $w_2 = 315$ nm (gray lines). The full (broken) lines are for **M** pointing to the right (left). [A positive (negative) field H points to the right (left).] The low-frequency (high-frequency) branches belong to the families of modes $n = 0$ ($n = 2$). The field dependencies are calculated following Ref. 18. (b) Four different configurations labeled I–IV of **H** and **M** for sample A. Letters I–IV in (a) refer to these configurations. (c) Crossing fields for Case III in (a) calculated as a function of width difference Δw for $w_1 = w_2 + \Delta w$ and $w_2 = 315$ nm. Symbols denote the respective fields H_{mr} (absolute values) for samples A and B.

given by the two panels I and IV in Fig. 3(b). However, when neighboring wires are magnetized in an antiparallel manner, the slopes $\partial f/\partial H$ of the respective $f(H)$ characteristics are of opposite signs for the two types of wires, since for the wires magnetized in the negative direction the $f(H)$ dependencies are falling [broken lines in Fig. 3(a)]. Thus, field-dependent resonances of the oscillators can now cross. The field position H_{cr} of a crossing depends on the magnetization configuration: It is either at a negative field [AFO state II in Fig. 3(b)] or a positive field [AFO state III in Fig. 3(b)]. The sign of H_{cr} is found to reflect the direction of **M** in the wide wires. In Fig. 3(c) we show the calculated variation in $|H_{cr}|$ with Δw for modes $n = 0$ and 2. We assume $w_1 = 315$ nm $+ \Delta w$. The fields H_{cr} for branch crossings shift to larger values with increasing Δw. We also place the experimentally measured fields H_{mr} for $n = 0$ and $n = 2$ into the picture (symbols). Strikingly, we find that the field positions $|H_{mr}|$ taken from Fig. 2(d) coincide with the calculated field positions H_{cr} of *crossing branches* predicted for *uncoupled* wires of width $w_1 = 370$ nm and $w_2 = 315$ nm. The measured fields $H_{mr,0}$ and $H_{mr,2}$ of sample B with $\Delta w = 0$ agree well also.[24]

B. Results from the micromagnetic simulations

Simulated spin-wave spectra for the FMO state of sample A are shown in Fig. 4(a). We find resonance pairs $n = 0,2,4\ldots$ of positive slopes $\partial f/\partial H$. Each pair consists of resonances where the lower-frequency (higher-frequency) one has a strong (weak) intensity. This agrees with the experimental data shown in Fig. 2(c) for $\mu_0 H > -10$ mT. We will focus on two pairs at small frequencies and label them with $(n = 0,a)$, $(n = 0,b)$, $(n = 2,a)$, and $(n = 2,b)$. In Figs. 4(b)–4(e) we show simulated spin precession profiles across the unit cell for these four resonances. At $H = 0$ we find a large spin precession amplitude in the wide (narrow) wire for $(n = 0,a)$ [$(n = 0,b)$]. For each of these resonances the other wire of the unit cell is less excited by h_{rf}. Note that in Figs. 4(d) and 4(e) the large spin precession amplitude remains located in one and the same wire of the unit cell for the whole range of H. Inside each wire there is just a single wave crest. The spin precession profiles resemble confined DE spin waves with no nodal plane which identifies them as $n = 0$ modes (consistent with our labeling). The fact that the wires of different width in the unit cell both exhibit a considerable spin precession amplitude at the same frequency is a sign of dipolar interaction between them. Note that the frequency separation between modes of the individual wires is predicted to be as large as 0.5 GHz which is large if compared to the linewidth of the individual resonances. In the noninteracting case there would be no frequency overlap. Thus, for uncoupled (i.e., noninteracting) wires one would expect a noticeable spin precession amplitude only in one of the wires, because the resonance frequencies differ for uncoupled wires due to the difference in widths [Fig. 3(a)] [c.f. Fig. 4 in Ref. 11]. Importantly, the collective resonances in Figs. 4(d) and 4(e) differ by the value of phase difference (not shown): For the mode at the lowest frequency $(n = 0,a)$ the oscillations in both wires are in-phase. For the mode $(n = 0,b)$ the oscillations are antiphase. This is a signature of hybridization of the resonance modes of individual wires: The dipolar interaction creates a doublet which consists of an acoustic (in-phase oscillation) and

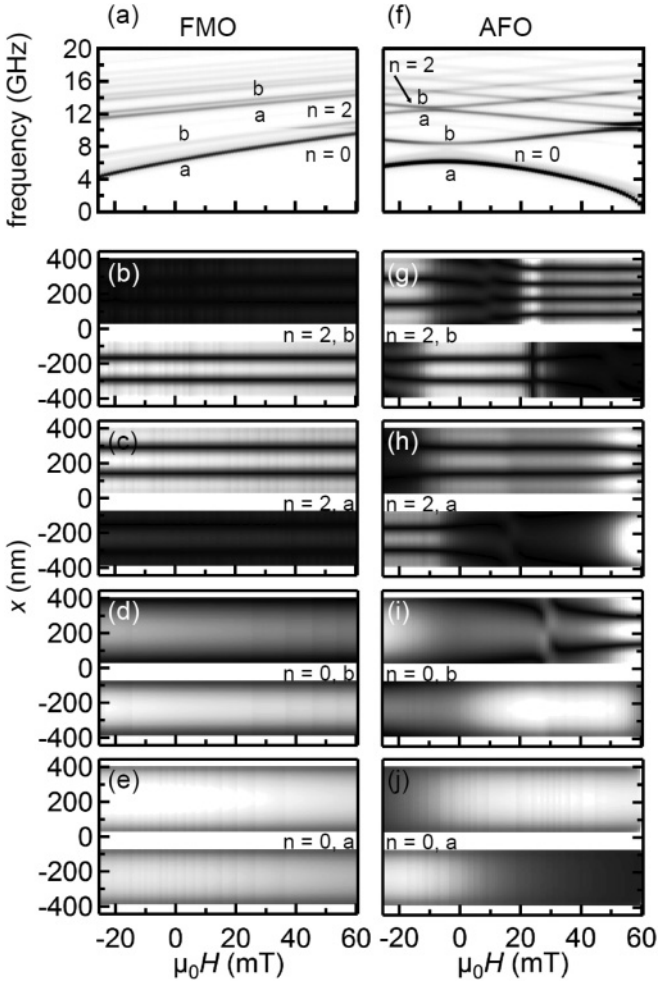

FIG. 4. (a) Field dependence of eigenfrequencies f simulated for sample A in the ferromagnetic order (FMO) state. Black color indicates spin-wave resonances. (b)–(e) Corresponding spin precession amplitudes for the two resonance pairs $n = 0$ and $n = 2$ across the width of the wires. Black (light gray) denotes a zero (large) precession amplitude. The white horizontal stripes mark the nonmagnetic space between nanowires. We show the variation of spin precession amplitudes as a function of applied field H. (f) Eigenfrequencies f in the antiferromagnetic order (AFO) state and (g)–(j) spin precession profiles for the modes as indicated in the graphs. In (a) and (f) the contrast in the grayscale plots is increased for $f > 10$ GHz. In (b)–(e) and (g)–(j) the wide wire is at the top of each graph. Note that the labeling n given in the right panels refer to the situation around $\mu_0 H_{\mathrm{mr},0} = -5$mT. In general, the panels illustrate the profiles attributed to the fourth (g), third (h), second (i), and first (j) branch of Fig. 4(f) if the resonances at a given field are numbered by one to four starting from the one of lowest frequency for each value of H given on the x axis.

optical (antiphase oscillation) mode. The antiphase oscillation provides the smaller integral signal due to a smaller net magnetic moment and a smaller net dynamical stray field. In Figs. 4(b) and 4(c) we display the behavior of $(n = 2,b)$ and $(n = 2,a)$, respectively, where nodal lines occur in the spin precession profiles. Again one finds that the large spin precession amplitude is in the wide (narrow) wire for the lower-frequency (higher-frequency) branch. We do not discuss and observe modes with $n = 1,3,\ldots$ due to the symmetry of the excitation field in the simulation and experiment.

In Fig. 4(f) we show simulated spectra for the AFO state of sample A. In the simulation the state is stable over a wider field range than in the experiment. Field-dependent spin-wave profiles are depicted in Figs. 4(g)–4(j). The spectra are very different from the ones of the FMO state and display a number of mode repulsions. The field $\mu_0 H_{\mathrm{mr},0}$ is found to be -5 mT consistent with the experiment. The splitting δf between $(n = 0,a)$ and $(n = 0,b)$ at $\mu_0 H_{\mathrm{mr},0} = -5$ mT amounts to 2.2 GHz. Note that the labeling n given in Figs. 4(g)–4(j) refer to the situation around $\mu_0 H_{\mathrm{mr},0} = -5$mT. This is the field regime which we focus on. At large positive fields the simulations predict further avoided crossings between higher order modes. These interesting features rest to be explored experimentally. Here the labeling would be different. In our sample the AFO state was not stable in this field regime of large positive H and we will not discuss such avoided crossings.

We analyze the mode $(n = 0,a)$ in Fig. 4(j) and find that the precession amplitudes are almost the same for the two wires of the unit cell at $\mu_0 H = \mu_0 H_{\mathrm{mr},0} = -5$mT. Both modes $(n = 0,a)$ and $(n = 0,b)$ near $H_{\mathrm{mr},0}$ are characterized by a single wave crest in each wire (i.e., they originate from the standing spin waves with no nodes). As for the FMO state, the modes $(n = 0,a)$ and $(n = 0,b)$ differ in their relative phase of the precessional motion. The lowest-frequency mode $(n = 0,a)$ is characterized by an in-phase (out-of-phase) oscillation of the in-plane (out-of-plane) magnetization component. The next higher-frequency mode $(n = 0,b)$ experiences an out-of-phase (in-phase) oscillation of the in-plane (out-of-plane) magnetization component. This complex behavior originates from the antiparallel alignment of $\mathbf{M}$ in neighboring wires and the dipolar coupling [c.f. Fig. 3(b) in Ref. 6]. At $\mu_0 H_{\mathrm{mr},0} = -5$ mT both modes can be seen as the in-phase and out-of-phase combinations of two individual DE spin waves $n = 0$ in neighboring wires. When dipolarly coupled they form a doublet consisting of an acoustic and optical mode, respectively. The dipolar interaction pushes the frequency of the optical mode upward and of the acoustic one downward with respect to the case of uncoupled wires. The frequency splitting δf arises. Since the in-plane component of precession amplitude is larger than the out-of-plane component the in-plane phases define the acoustic and optical modes. The large ellipticity of precession of the magnetization in high magnetic moment metallic films results in a much larger amplitude of the in-plane component of the dynamic magnetization than the out-of-plane one. As follows from the formalism in Ref. 18 the dynamic stray fields produced by both components are of the same shape and their magnitudes scale linearly with the amplitude of the respective components of dynamic magnetization. The scaling factor is the same for both field components. Consequently, the stray field which is induced by the in-plane component is much stronger and is mostly responsible for the dynamic dipolar coupling of the wires. This is why the phases of the in-plane precessional components are considered to define the assignment of acoustic and optical modes.

If we follow the mode profile $(n = 0,a)$ in Fig. 4(j) to more negative (positive) values of H, we find that the spin precession amplitude grows in the narrow (wide) wire. Strikingly, one sees

an opposite behavior in Fig. 4(i) around $H_{mr,0}$ for $(n = 0,b)$. Comparing modes $(n = 0,a)$ and $(n = 0,b)$ as a function of H we find that for the wide wire the mode $(n = 0,b)$ shows a large precession amplitude in the field range from -30 to -5 mT [Fig. 4(i)]. Above $H_{mr,0} = -5$mT the amplitude decreases. In this field range the mode $(n = 0,a)$ acquires the largest amplitude for the wide wire. For the narrow wire the scenario of interchanging spin precession amplitudes is opposite. This difference between Figs. 4(i) and 4(j) evidences that the two fundamental modes $n = 0$ of the individual wires are hybridized and follow an avoided crossing behavior as a function of H. For the resonance pair $n = 2$ mode repulsion is predicted for $H_{mr,2} = -9$ mT [Figs. 4(g) and 4(h)]. Here the frequency splitting is only 0.3 GHz and much smaller if compared with $n = 0$. The simulations predict further mode repulsions centered at $+33$ and $+55$ mT. They have not been accessible in the experiment as the wires in the real sample switch to the FMO state at a smaller field.

The simulated frequency splitting of $\delta f = 2.2$ GHz for $n = 0$ is larger by about 1 GHz than the experimentally observed one. This points to an overestimation of the strength of the dipolar interaction between spin waves in neighboring wires. We will address this point later.

C. Solutions of the integro-differential equation from the linearized Landau-Lifshitz-Gilbert equation

In Fig. 5 we compare the experimental data obtained on sample A (symbols) with the theory using the dipolar coupling length l_c as a fit parameter. One sees that for the FMO state (straight lines) the agreement with the experiment is excellent assuming $l_c = 2.4$ μm. The value is similar if compared to the results obtained on sample B in Ref. 6. The agreement for the AFO state (curved lines) is good for negative field values. It noticeably worsens for positive H. Importantly, the experimental data for positive H are close to the theoretical line for the FMO state. In Ref. 7 this observation was also made and explained as the influence of a small ferromagnetic domain dipolarly coupled to the AFO environment.

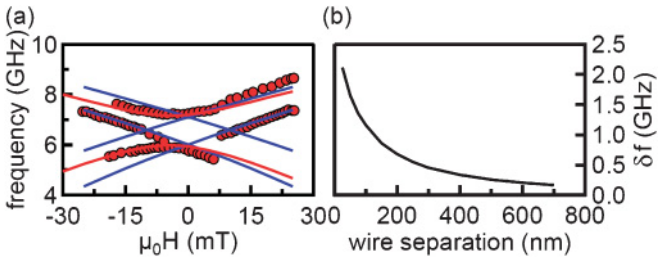

FIG. 5. (Color online) (a) Comparison of experimental (symbols) and theoretical data (lines) for sample A. Straight lines which cross represent the eigenfrequencies calculated for the FMO state where we consider the two possible and opposite orientations of the saturation magnetization. The curved lines displaying the field-dependent mode repulsion indicate the calculated eigenfrequencies of the AFO state. We consider a dipolar coupling length l_c of 2.4 μm. Circles are the resonance positions extracted from the experimental data of Fig. 2(d) for $n = 0$. (b) Frequency splitting δf for the AFO state as a function of the edge-to-edge separation between the wires.

Following Fig. 5 a reduced dipolar coupling length l_c allows us to explain the smaller frequency splitting δf observed in the experiment if compared to the micromagnetic simulations. Here we note that there is no adjustable parameter in exact micromagnetic models which would reduce δf without affecting the frequency positions for all the higher-order modes. The only parameter is the length (strength) of the dipolar coupling which affects the magnonic band bandwidth and therefore δf without noticeably affecting the frequency positions of the higher-order modes being less dispersive by themselves. The higher-order modes are less affected by the finite l_c because the nodal lines introduce phase shifts inside each nanowire which reduce the dynamic stray field due to internal compensation. The dynamic dipolar coupling of higher-order modes is intrinsically much smaller. In general, the dipolar coupling is completely determined by the array geometry. In Ref. 5 it was suggested that the systematic discrepancy observed in the low-frequency resonance pair $n = 0$ originated from imperfections of the geometry of the real artificial crystal. Imperfections in the lithography might have provoked a deviation from the perfect periodicity. It was proposed that the imperfections may result in a reduction of the collective dynamic stray field and thus in a decrease in the dynamic dipolar coupling. Analysis of the effect of specific imperfections on δf is out of the scope of the present paper.

Using the same theory we made further numerical calculations of the frequency splitting δf between the acoustic and optical mode of the $n = 0$ pair for the AFO state. On the one hand we calculated δf as a function of the difference Δw of the wire widths introduced in Fig. 3(b). For each Δw we determined the value $H_{mr,0}$ and then extracted δf at this field position. We found that the frequency splitting varied only slightly when we changed Δw from 0 to 100 nm. δf decreased by just 0.05 GHz from 1.21 to 1.16 GHz (not shown). At the same time the field $H_{mr,0}$ varied by several mT. On the other hand we calculated δf as a function of the distance between wires of $w_1 = 315$ nm and $w_2 = 370$ nm considering $l_c = 2.4$ μm. In Fig. 5(b) we find that the frequency splitting decreases considerably with increasing edge-to-edge separation a at small separations. At large a the splitting δf approaches zero. At a few 100 nm the wire separation is so large that the dipolar coupling of wires becomes negligible. This is one more evidence of the fact that the frequency splitting originates from the hybridization of resonances in the wide and narrow nanowires.

VI. CONCLUSIONS

We investigated densely packed arrays of narrow $Ni_{80}Fe_{20}$ wires where a small edge-to-edge separation created an appreciable dipolar coupling between individual wires. Using broadband spectroscopy we investigated the spin waves in the long-wavelength limit. In particular we focused on an array consisting of wires of two different widths $w_1 = 370$ and $w_2 = 315$ nm and analyzed in particular antiferromagnetic alignment of neighboring wires. The edge-to-edge separation a was 100 nm. Consistent with a previous study[6] conducted for a width difference $\Delta w = 0$, we observed a nonmonotonic behavior of eigenfrequencies f as a function of the in-plane magnetic field H. We found two characteristic modes which

exhibited a mode repulsion behavior. Using micromagnetic simulations and theoretical modeling we attribute this to a geometry- and field-controlled avoided crossing of confined nanowire modes. The frequency splitting δf is minimal for a field H_{mr} where spin-wave frequencies f of *uncoupled* wires with opposite orientations of magnetization **M** are degenerate. Dynamic dipolar coupling of the oscillators removes this degeneracy and leads to the frequency splitting between acoustic and optical modes. The splitting δf and field H_{mr} are found to depend crucially on the edge-to-edge separation a and width difference Δw, respectively. These properties are thus controlled by nanolithography. This provides a further means to tailor the frequency response of magnonic crystals which are relevant for future magnonic applications.

ACKNOWLEDGMENTS

We acknowledge financial support from the DFG via SFB 668, "Nanosystems Initiative Munich," City of Hamburg via "Nano-Spintronics," Australian Research Council and European Community's Seventh Framework Programme (FP7/2007-2013) under Grant Agreement No. 228673 (MAGNONICS). We thank Sebastian Hankemeier for making the MOKE measurements possible.

*grundler@ph.tum.de

[1] J. Jorzick, S. Demokritov, C. Mathieu, B. Hillebrands, B. Bartenlian, C. Chappert, F. Rousseaux, and A. Slavin, Phys. Rev. B **60**, 15194 (1999).

[2] J. Jorzick, S. Demokritov, B. Hillebrands, M. Bailleul, C. Fermon, K. Y. Guslienko, A. N. Slavin, D. V. Berkov, and N. L. Gorn, Phys. Rev. Lett. **88**, 047204 (2002).

[3] C. Kittel, Phys. Rev. **73**, 155 (1948).

[4] F. Giesen, J. Podbielski, T. Korn, M. Steiner, A. van Staa, and D. Grundler, Appl. Phys. Lett. **86**, 112510 (2005).

[5] G. Gubbiotti, S. Tacchi, M. Madami, G. Carlotti, S. Goolaup, A. O. Adeyeye, and M. P. Kostylev, J. Phys. D: Appl. Phys. **43**, 264003 (2010).

[6] J. Topp, D. Heitmann, M. Kostylev, and D. Grundler, Phys. Rev. Lett. **104**, 207205 (2010).

[7] J. Ding, M. Kostylev, and A. O. Adeyeye, Phys. Rev. B **84**, 054425 (2011).

[8] V. V. Kruglyak, S. O. Demokritov, and D. Grundler, J. Phys. D: Appl. Phys. **43**, 264001 (2010).

[9] J. Topp, J. Podbielski, D. Heitmann, and D. Grundler, Phys. Rev. B **78**, 024431 (2008).

[10] J. Topp, D. Heitmann, and D. Grundler, Phys. Rev. B **80**, 174421 (2009).

[11] J. Topp, G. Duerr, K. Thurner, and D. Grundler, Pure Appl. Chem. **83**, 1989 (2011).

[12] S. Tacchi, M. Madami, G. Gubbiotti, G. Carlotti, S. Goolaup, A. O. Adeyeye, N. Singh, and M. P. Kostylev, Phys. Rev. B **82**, 184408 (2010).

[13] J. Podbielski, F. Giesen, M. Berginski, N. Hoyer, and D. Grundler, Superlattices Microstruct. **37**, 341 (2005).

[14] S. Kalarickal, P. Krivosik, M. Wu, and C. E. Patton, J. Appl. Phys. **99**, 093909 (2006).

[15] J. Podbielski, D. Heitmann, and D. Grundler, Phys. Rev. Lett. **99**, 207202 (2007).

[16] G. Woltersdorf and C. H. Back, Phys. Rev. Lett. **99**, 227207 (2007).

[17] V. E. Demidov, M. Buchmeier, K. Rott, P. Krzysteczko, J. Münchenberger, G. Reiss, and S. O. Demokritov, Phys. Rev. Lett. **104**, 217203 (2010).

[18] K. Y. Guslienko, S. O. Demokritov, B. Hillebrands, and A. N. Slavin, Phys. Rev. B **66**, 132402 (2002).

[19] M. Donahue and D. G. Porter, *OOMMF User's Guide, Version 1.0, Interagency Report NISTIR 6376*, Tech. Rep. (National Institute of Standards and Technology, Gaithersburg, 1999).

[20] K. M. Lebecki, M. J. Donahue, and M. W. Gutowski, J. Phys. D: Appl. Phys. **41**, 175005 (2008).

[21] J. Ding, M. Kostylev, and A. O. Adeyeye, Phys. Rev. Lett. **107**, 047205 (2011).

[22] S. Goolaup, A. O. Adeyeye, N. Singh, and G. Gubbiotti, J. Appl. Phys. **103**, 07D528 (2008).

[23] R. D. McMichael and B. B. Maranville, Phys. Rev. B **74**, 024424 (2006).

[24] For an array of perfect antiferromagnetic order one would expect $H_{\mathrm{mr},0} = H_{\mathrm{mr},2} = 0$. We observed $H_{\mathrm{mr},0}$ between -1 and -2 mT most likely due to remaining subdomains in the FMO state self-biasing the array.[6]